Assessment of biomass burning smoke influence on environmental conditions for multi-year tornado outbreaks by combining aerosol-aware microphysics and fire emission constraints

Pablo E. Saide (1), Gregory Thompson (2), Trude Eidhammer (2), Arlindo M. da Silva (3), R. Bradley Pierce (4) and Gregory R. Carmichael (5)

(1) Advanced Study Program and Atmospheric Chemistry Observations and Modeling Lab, National Center for Atmospheric Research, Boulder, Colorado, USA.

(2) Research Applications Laboratory, National Center for Atmospheric Research, Boulder, Colorado, USA.

(3) Global Modeling and data Assimilation Office, NASA Goddard Space Flight Center, Greenbelt, Maryland, USA.

(4) NOAA Satellite and Information Service (NESDIS) Center for Satellite Applications and Research (STAR), Madison, Wisconsin, USA.

(5) Center for Global & Regional Environmental Research, University of Iowa, Iowa City, Iowa, USA.

Correspondence to: P. E. Saide (saide@ucar.edu)

Key Points

- WRF with aerosol-aware microphysics is used to study smoke impacts on multiple tornado outbreaks

20   • Although smoke is always present, changes in environmental conditions due to smoke are

21   highly variable

22   • WRF and WRF-Chem simulations can produce similar AOD and smoke impacts

23

24   **Abstract**

25   We use the WRF system to study the impacts of biomass burning smoke from Central America

26   on several tornado outbreaks occurring in the US during spring. The model is configured with an

27   aerosol-aware microphysics parameterization capable of resolving aerosol-cloud-radiation

28   interactions in a cost-efficient way for numerical weather prediction (NWP) applications.

29   Primary aerosol emissions are included and smoke emissions are constrained using an inverse

30   modeling technique and satellite-based AOD observations. Simulations turning on and off fire

31   emissions reveal smoke presence in all tornado outbreaks being studied and show an increase in

32   aerosol number concentrations due to smoke. However, the likelihood of occurrence and

33   intensification of tornadoes is higher due to smoke only in cases where cloud droplet number

34   concentration in low level clouds increases considerably in a way that modifies the

35   environmental conditions where the tornadoes are formed (shallower cloud bases and higher

36   low-level wind shear). Smoke absorption and vertical extent also play a role, with smoke

37   absorption at cloud-level tending to burn-off clouds and smoke absorption above clouds resulting

38   in an increased capping inversion. Comparing these and WRF-Chem simulations configured with

39   a more complex representation of aerosol size and composition and different optical properties,

40   microphysics and activation schemes, we find similarities in terms of the simulated aerosol

41   optical depths and aerosol impacts on near-storm environments. This provides reliability on the

42 aerosol-aware microphysics scheme as a less computationally expensive alternative to WRF-

43 Chem for its use in applications such as NWP and cloud-resolving simulations.

44

1. Introduction

46 Numerical weather prediction (NWP) is routinely used by forecasters as a tool (among many

47 others) to warn the population of possible severe weather events and is thought to be at least

48 partially responsible for a decrease in death tolls during tornado outbreaks (Brooks and Doswell,

49 2002). When building convective outlooks and issuing "Tornado Watches", NWP is generally

50 used to forecast the environmental conditions that are favorable for the formation of tornadoes.

51 These conditions include high low-level wind shear, storm-relative helicity (SRH) and

52 convective-available potential energy (CAPE); and low lifting condensation level (LCL, roughly

53 the cloud base height), which are often combined in composite parameters (e.g., Significant

54 Tornado Parameter (STP)) to provide a combined score (Rasmussen and Blanchard, 1998;

55 Thompson et al., 2003). Recent studies have begun analyzing the influence of large-scale

56 phenomena such as the Madden-Julian Osciallation (Barrett and Gensini, 2013) and climate

57 change (Brooks, 2013; Diffenbaugh et al., 2013) on these precursor atmospheric conditions

58 common to tornado days. The mechanisms through which these environmental conditions are

59 connected to tornado genesis, longevity, and intensity have been hypothesized (Markowski and

60 Richardson, 2009), but remain as open questions. However, as forecasts of these conditions have

61 shown skill on predicting severe weather outbreaks (e.g., Hamill et al., 2005; Knupp et al.,

62 2013), a continuous effort to improve these forecasts further is needed.

63   Aerosols can interact with clouds and solar radiation and modulate climate (Boucher et al.,

64   2013). The inclusion of these interactions into NWP can impact forecasts (e.g., Kolusu et al.,

65   2015). Convective-scale weather prediction models are moving towards the inclusion of these

66   interactions by the use of aerosol-aware microphysics that incorporate aerosols explicitly in a

67   simple and cost-effective manner (Lebo and Morrison, 2013; Thompson and Eidhammer, 2014).

68   More complex schemes that resolve atmospheric chemistry and represent the size and

69   composition distributions of aerosols with greater detail (e.g., Eidhammer et al., 2014) are

70   currently too computationally expensive to be used in operational high-resolution forecasts. A

71   comparison between these two types of schemes could be performed to assess how aerosols may

72   impact specific weather phenomena and how much complexity in aerosol treatment may be

73   warranted for future operational NWP.

74   Biomass burning aerosol (smoke) is estimated to be the major contributor to the global burden of

75   fine carbonaceous aerosols (Andreae and Rosenfeld, 2008; Bond et al., 2004) and to significantly

76   influence climate (Jacobson, 2014). In particular, smoke from fires in Central America has been

77   shown to be in the inflow of severe weather in the US and has been hypothesized to intensify the

78   outbreaks by the convective invigoration mechanism (Wang et al., 2009). Saide et al. (2015b)

79   found that Central American smoke was capable of intensifying tornado outbreaks by lowering

80   LCL and increasing low level shear. This is achieved through two pathways: 1) optical

81   thickening of shallow clouds present before the outbreak which reduce downward solar radiation

82   at the surface stabilizing the boundary layer, and 2) enhancement of the capping inversion by

83   heating of the layer above cloud by soot absorption (Saide et al., 2015b). These studies focused

84   on specific outbreaks and there has been no assessment of these aerosol-associated impacts for

85   multiple outbreaks on multiple years.

86   This study intends to advance our understanding on the interactions of smoke with severe

87   weather and to help transition the inclusion of fully-coupled aerosol-cloud-radiation interactions

88   into NWP. To do so, we compare simple and complex treatments of these interactions in the

89   Weather Research and Forecasting (WRF) and WRF-Chem systems, explore the influence of

90   smoke presence on tornado outbreaks occurring in multiple years, and evaluate the relevance of

91   the proposed mechanism proposed in Saide et al. (2015b) in these outbreaks (Section 3).

92   Furthermore, biomass burning emissions have been found to have large uncertainties; for

93   instance, Kaiser et al. (2012) found that a factor of three increase in smoke emissions is needed

94   to improve agreement with observations, while Zhang et al. (2014) found discrepancies of up to

95   a factor of 10 between various smoke emission estimates. Thus, to reduce these uncertainties, in

96   this study biomass burning emissions are constrained for each outbreak with satellite-based

97   aerosol optical depth (AOD) retrievals using a recently developed algorithm (Saide et al., 2015a).

98   The next section describes details on the tornado outbreaks studied, the modeling framework and

99   the inversion algorithm. Section 3 contains results and discussion about the emission inversions

100   and smoke presence and impacts during outbreaks, while in the last section we provide

101   conclusions and future directions.

102   **2. Methods**

103   2.1. Tornado Outbreaks studied

104   We selected eight major tornado outbreaks between 2003 and 2014. This period was chosen due

105   to availability of data from the Moderate Resolution Imaging Spectroradiometer (MODIS) on

106   both Terra and Aqua satellites (operational from mid-2002 to date) as fire emissions and AOD

107   retrievals used herein are based on the MODIS products (see next sections). Only episodes

108   occurring during April and May (not including those very early and very late in each month,

109   respectively) were chosen to coincide with the strongest biomass burning in Central America

110   (Reid et al., 2004). The tornado tracks of the outbreaks selected are shown in Figure 1 and

111   represent locations across the Southeast, Midwest and Southwest United States (US). Other

112   selection criteria were for each outbreak to contain at least four tornadoes of EF2 scale or greater

113   (to filter out the less significant outbreaks), the tornados were not so broadly spread in order that

114   model simulations would fit reasonably within a nested domain, and the most severe and more

115   numerous tornadoes needed to occur in the afternoon or early evening. The latter condition is

116   imposed because the proposed mechanisms being studied are driven by peak solar heating, which

117   would dissipate at night or not yet occur in the morning. Many of these outbreaks have been

118   highlighted as major events of the year they occurred (Blunden and Arndt, 2012, 2014, 2015;

119   Levinson and Lawrimore, 2008; Levinson and Waple, 2004; Peterson and Baringer, 2009) and

120   specific studies have focused on their characteristics and impacts (Hamill et al., 2005; Knupp et

121   al., 2013). The environmental conditions provided by Storm Prediction Center (SPC)

122   Convective Outlooks and Mesoscale Analysis for these outbreaks are shown in Figure 2.

123   2.2. Regional modeling

124   We use two configurations of the WRF system to perform simulations of aerosols and their

125   impacts on weather, one with the Thompson and Eidhammer (2014; hereafter referred to as

126   TE2014) aerosol-aware microphysics (AAM) scheme and the other with WRF-Chem.

127   The TE2014 aerosol-aware microphysics consists of a double-moment bulk microphysical

128   parameterization that explicitly resolves droplet nucleation and ice activation due to aerosols.

129   Besides cloud water, cloud ice, snow, graupel, and rain hydrometeor species, the scheme

130 transports two aerosol species (hygroscopic and ice-nucleating) adding only about 15%

131 computational cost, therefore making it suitable for NWP applications. Aerosol-radiation

132 interactions were recently included to the AAM configuration by computing AOD at 550 nm

133 based on the two aerosol species using a look-up table procedure to include aerosol hygroscopic

134 growth. Then, spectral AOD and other aerosol optical properties (AOPs) such as Angstrom

135 exponent, single-scattering albedo and asymmetry factor are parameterized following the

136 methods of Ruiz-Arias et al. (2014) considering a rural type aerosol. These spectral AOPs are

137 then used in the Rapid Radiative Transfer Model for climate and weather models (RRTMG)

138 shortwave radiation parameterization (Iacono et al., 2008).

139 While TE2014 used a constant flux derived from initial aerosol concentrations to represent

140 emission processes, we modified WRF-Chem emission routines to include primary-aerosol

141 number emissions explicitly into the aerosol-aware microphysics parameterization. The

142 MOSAIC aerosol scheme (Zaveri et al., 2008) in WRF-Chem can solve aerosol mass and

143 number for 8 sectional size bins. Thus, emission routines coupled to this scheme (anthropogenic,

144 fires, dust and sea-salt) provide aerosol number per size bin, which were summed up to obtain

145 total aerosol number concentrations needed by the TE2014 scheme. We used biomass burning

146 emissions produced by the Quick Fire Emission Dataset (QFED) v2.4 (Darmenov and da Silva,

147 2015) which were included into the model using the WRF-Chem online plume rise model (Grell

148 et al., 2011). Anthropogenic emissions correspond to NEI 2005

149 (http://www.epa.gov/ttnchie1/net/2005inventory.html) for the US, 1999 Mexico emissions

150 described in Mena-Carrasco et al. (2009) updated to 2012 using growth factors from Wolf et al.

151 (2009), and emissions derived with PREP-CHEM-SRC code (Freitas et al., 2011) for the rest of

152 Central America. Sea-salt and dust emissions were estimated online by using the Gong et al.,

153 (1997) and Zhao et al. (2010) parameterizations, respectively. Although secondary aerosol

154 production is not modeled (no chemical mechanism used and no gaseous species modeled), it

155 should not affect aerosol number concentration significantly as secondary aerosol is expected to

156 condense on already existing particles. Aerosol boundary conditions are provided every 6 hours

157 by global simulations of MOZART (Emmons et al., 2010), while initial conditions are obtained

158 from the monthly climatology derived by Thompson and Eidhammer (2014). The month when

159 the simulation was started was used as initial condition when fire emissions were included, while

160 February was used for simulations without fire emissions to provide a smoke-free initialization.

161 As in TE2014, only dust was considered to be ice nucleating while all other aerosol species

162 (except black carbon) were apportioned to the hygroscopic aerosol. Although black carbon is not

163 apportioned, the two aerosol species are considered to absorb solar radiation as mentioned above.

164 WRF-AAM was configured for each tornado outbreak by using two domains of 12 km and 4 km

165 grid-spacing. The outer domains covered roughly between -110° and -75° longitude for all

166 outbreaks, and from 10° to 50° latitude for outbreaks in 2007 and 24 May 2008 and from 10° to

167 45° latitude for the rest of the outbreaks (Fig. 3). The inner domains are shown in Figure 1 and

168 were designed to include each outbreak region. All simulations were initialized at 00 UTC seven

169 days prior to the outbreak studied to provide spin-up time for aerosol concentration and

170 feedbacks to meteorology. Meteorological initial and boundary conditions were obtained from

171 NCEP final analysis (NCEP, 2000). Other WRF configuration choices include RRTMG long-

172 wave radiation (Iacono et al., 2000), MYJ boundary layer (Janjić, 2002), Noah land surface

173 model (Barlage et al., 2010), GF cumulus scheme (Grell and Freitas, 2013) for the 12 km domain

174 and no convective parameterization was used for the 4 km domain. Figure 2 compared to Figure

175 4 shows that the model configured this way is able to represent the tornadic environment found

176 on all outbreaks, although some shifts in the maximum values are often found which is expected

177 due to the long spin-up used.

178 The WRF-Chem configuration used is the same as the one described in Saide et al. (2015b)

179 unless noted differently here. For consistency between simulations, WRF-Chem uses the same

180 configuration as WRF-AMM, including domains, vertical and horizontal resolution, emission

181 databases, initial and boundary conditions, and physics configuration, excluding the

182 microphysics and aerosol activation parameterizations where the Morrison and Abdull-Razak

183 and Ghan schemes are used (Abdul-Razzak and Ghan, 2002; Yang et al., 2011 and references

184 therein). The chemical mechanism and aerosol models correspond to the CBMZ (Zaveri and

185 Peters, 1999) and 8 size bin MOSAIC (Zaveri et al., 2008).

186 2.3. Inversion scheme

187 The algorithm described in Saide et al. (2015a) is used to constrain biomass burning emissions

188 for each outbreak studied. The algorithm requires the use of two WRF simulations, one with

189 first-guess (or initial) emissions (QFED in this case) and another one with perturbed emissions.

190 As assessing smoke impacts involves performing simulations with and without fire emissions

191 (Saide et al., 2015b), the perturbed simulation is chosen as the one with the fire emissions turned

192 off (i.e., perturbation factor equals zero). This reduces the computational burden because the

193 perturbation simulation is used both for the inversion step and for assessing the smoke effects.

194 Also, the simulations need to produce estimates of the observation used to constrain emissions,

195 which in this case is AOD and can indeed be estimated by WRF-AAM (see previous section).

196 Additionally, the simulations used in the inversion algorithm need to solve for tracers tagged to

197 the emissions being constrained. These tracers provide the emission's footprint in the

198   observation location and are used to derive the sensitivities (derivatives) used in the inversion

199   scheme. In this study the tracers are tagged to fire emissions from four regions, every six hours

200   and during eight day simulations, resulting in 128 tracers. The four regions are shown in Figure 5

201   and correspond roughly to the east (1) and west (2) of the Mexican Central Plateau, (3) the

202   Yucatan peninsula including Belize and Guatemala, and (4) the rest of Central American

203   countries to the south. The tracers are modeled only on the 12 km domain as here is where the

204   inversion is performed.

205   The variational inversion algorithm determines the optimal scaling factors to be applied to the

206   fire emissions. A cost function with two terms is minimized to (1) improve model fit to the

207   observations but at the same time (2) do not exceedingly deviate from the initial guess estimate.

208   We use the same parameters as in Saide et al. (2015a) to weight these two terms with the

209   exception of the length scale to correlate emissions temporally, which is changed from 4 to 6

210   hours. This choice of parameters provides a good fit to the data with little bias and produces

211   large deviations from the highly uncertain guess emissions, but does not generate very steep

212   temporal changes in the correction factors. Finally, one more simulation is performed with the

213   constrained emissions, and this simulation is compared to the one without fire emissions to

214   assess the smoke impacts. These two simulations (constrained fire emissions and no fires) use

215   the two domains (12 km and 4km resolution) and comparisons are performed on the inner

216   domain only. The inversions are performed only for the WRF-AAM configurations, while WRF-

217   Chem configurations using constrained smoke emissions use the ones obtained from WRF-AAM

218   inversions corresponding to the same episode.

219   We use observed AOD at 550 nm from the NASA neural-network retrieval (NNR, GMAO,

220   2014; Saide et al., 2013) to constrain emissions, which are assimilation-grade retrievals based on

221 MODIS products calibrated to match Aerosol RObotic NETwork (AERONET) AOD data

222 (Holben et al., 2001). Only NNR observations from -110° to -80° longitude, from 10° to 30°

223 latitude, and over 0.2 AOD are used in the inversion to avoid correcting fire emissions based on

224 retrievals far from the source region and not significantly influenced by fires.

225 2.4. Summary of simulations

226 We performed three WRF-AAM simulations for the eight outbreaks studied: 1) Fire emissions

227 turned off and two domains, 2) Initial fire emissions including tracers and only for the 12km

228 domain, and 3) Constrained emissions for the two domains. These sum up to 24 simulations.

229 Then, we performed various sensitivity simulations by turning off absorption and changing

230 initial smoke emissions (see section 3.4 for details) for three outbreaks. One simulation per

231 outbreak was performed for absorption effects (only #3 as fire off was already performed), while

232 two for the initial emissions sensitivity (#2 and #3 as the inversion needs to be repeated).

233 Together with the base-line simulations, this gives a total of 33 WRF-AAM simulations. We also

234 performed simulations #1 and #3 using WRF-Chem for three outbreaks, thus a total of 6 WRF-

235 Chem simulations (section 3.5). Additionally, one WRF-Chem simulation of type #2 but without

236 the tracers was performed to compare AOD against WRF-AAM. Note that each WRF-Chem

237 simulation is ~10 times more computationally expensive than the corresponding WRF-AAM.

238 **3. Results and discussion**

239 3.1. Inversion results

240 Figure 5 shows the daily emissions by region before and after the inversion for all outbreaks

241 studied when using the AAM configuration. Prior smoke emissions are found to be

242 underestimated for most times during all cases studied, with domain-wide emission scaling

11

243   factors in the range of 1.4-2.6, depending on the case. The corrections to the prior emissions tend

244   to vary substantially by region and by day, which shows that the choice of independently

245   constraining emissions by region and by time was appropriate. Figure 6 shows an example of

246   how the modeled AOD generally improves the fit with respect to the observations after

247   constraining emissions, indicating that the inversion algorithm is functioning properly. Although

248   there is overall improvement, some regions show degraded AOD after the inversion (e.g.,

249   southwest Mexico), which can happen because of the limited number of parameters being

250   optimized (4 regions, 4 times a day) and the large amount of data being ingested (i.e., the system

251   is over determined).

252   3.2. Smoke presence within outbreak regions

253   Figure 7 (top panels) shows the vertical distributions of aerosol number concentration in the

254   region of each outbreak studied, while Figure 8 shows the boundary layer height distributions.

255   We find that smoke contributes significantly to the total aerosol number concentration for all of

256   the outbreaks analyzed no matter the location of the outbreak. Smoke can be effectively

257   transported to the regions where outbreaks occur due to the southerly airflow from the Gulf of

258   Mexico during spring (Wang et al., 2006; Wang et al., 2009) and because of the low-level jet that

259   transports warm, moist air from the same region, which is a typical feature that triggers these

260   outbreaks (Hamill et al., 2005; Knupp et al., 2013). The vertical location of smoke can vary from

261   case to case; with all outbreaks showing smoke within the boundary layer and only some cases

262   (15 and 27 April 2011, 28 April 2014) presenting a thick smoke layer extending higher into the

263   lower troposphere (up to ~5 km). WRF-Chem simulations for the 27 April 2011 outbreak also

264   showed a thick layer of smoke (Saide et al., 2015b), which is consistent with the WRF-AAM

265   results and as expected because both model configurations use the same transport scheme.

266   CALIPSO provides observations of vertically resolved aerosols, which can be used to evaluate

267   the modeled vertical distribution of the smoke layer when the satellite overpasses it. Since the

268   regions where the outbreaks occur are generally cloudy, we performed the evaluation over the

269   Gulf of Mexico, which is the inflow region (Figure 3). We find the model generally reproduces

270   the layers observed by CALIPSO with skill and at a similar altitude, going from shallow layers

271   of smoke found on 28 April 2014 to layers up to ~6 km altitude on 15 April 2011. This shows

272   that the plume rise parameterization and the model transport are reliable, which increases the

273   confidence on the vertical distribution of smoke on the outbreaks regions shown on Figure 7.

274   3.3. Impacts on environmental conditions

275   The changes produced by the presence of smoke in near-storm environment conditions can be

276   obtained by comparing simulations with and without smoke emissions (Figure 9). Although

277   smoke is present in the outbreak region for all cases studied, the impacts of smoke on

278   environmental conditions vary by case. The outbreaks on 4 May 2003 and 27 April 2011 show

279   the largest and most consistent effects of smoke on LCL (~90-130 m reduction in mean), low-

280   level shear (1.5-2.2 m/s increase in mean) and SRH (30-80 m^2/s^2 increase in mean), with the

281   interquartile region showing values that produce an intensification of tornadic environments

282   (negative LCL and positive 1-km shear and SRH differences). Statistics of these variables for

283   multiple events have shown that differences in median between supercell types (non-tornadic to

284   weakly tornadic, and weakly to significantly tornadic) are ~-170 m, 1.7 m/s and ~30-45 m^2/s^2 for

285   LCL, low-level shear and SRH, respectively (Thompson et al., 2003). Thus, the smoke effects

286   shown here can reach magnitudes relevant for tornadogenesis and increase in tornado intensity.

287 Given that the statistics in Figure 9 are computed using a large number of grid-cells (7,000-

288 23,000 depending on the case), statistically significant differences are likely to be found even if

289 differences between simulations are small. Thus, instead of using *p-values*, we estimate the

290 magnitude of the difference between groups (effect size) using the standardized difference

291 (difference between means divided by the standard deviation of either group) and consider small,

292 medium, large, and very large values of this quantity equal to 0.2, 0.5, 0.8 and 1.3, respectively

293 (Sullivan and Feinn, 2012). As expected, the outbreaks on 4 May 2003 and 27 April 2011 show

294 medium to large effect size for LCL, 1km shear and SRH (Figure 9). While 10 May 2008, 15

295 April 2011 and 28 April 2014 generally show a small effect size, the rest of the outbreaks show

296 negligible effects of smoke. Although the 23 May 2008 and 19 May 2013 outbreaks show

297 positive LCL mean (i.e., a reduction in tornado likelihood due to smoke), this is found to be a

298 negligible effect size due to the large spread in these simulations.

299 Elevated CAPE and large-scale shear (6 km layer) are generally understood as a requirement for

300 supercell formation rather than an indicator to discriminate between tornadic categories

301 (Thompson et al., 2002; Thompson et al., 2003). Figure 9 shows the effects of smoke on these

302 two variables. For CAPE, although the outbreak on 4 May 2003 shows a very large increase in

303 CAPE due to smoke, the simulation without fires has mean CAPE of ~1500 J/kg which is high

304 enough to support the formation of supercells in the model (not shown). On the other hand, for

305 the 27 April 2011 outbreak there is only a medium effect size showing a decrease in CAPE due

306 to smoke. But again both simulations show mean CAPE of over 2000 J/kg, thus this difference is

307 not expected to impact supercell formation. On the other hand, all cases show a negligible effect

308 of smoke on 6km shear, which is different to the effects mentioned earlier for 1km shear. This

309 indicates that changes in wind due to smoke are mostly located in the lower layers. Figure 9 also

310   shows Convective Inhibition (CIN), which is also a parameter used to assess the formation of

311   supercells, indicating a small to negligible effect of smoke on this parameter. Although the

312   smoke produces stronger CIN (i.e, more negative) for the 4 May 2003 outbreak, supercells are

313   still generated in regions of close to zero CIN for the simulation including smoke emissions.

314   Why is there large variability in the smoke effects on environmental conditions although all

315   outbreaks studied consistently show smoke presence? Figure 7 shows cloud droplet number

316   concentrations (NDROP, middle panels) and cloud fraction (bottom panels) that can help answer

317   this question. For instance, 4 May 2003 and 5 May 2007 show similar patterns of smoke (mostly

318   contained in the boundary layer) and similar cloud fractions (ranging from 0.3 to 0.7 in the 0.25-

319   1.25 km layer). However, for 4 May 2003 the impacts of smoke on NDROP in the 0.25-1.25 km

320   layer are large (2-3 fold increase on average), while they are small for the 5 May 2007 outbreak

321   (50-67 % increase on average), which coincides with a large and negligible effect on

322   environmental parameters for the 4 May 2003 and 5 May 2007 outbreaks, respectively. One of

323   the mechanisms that generate conditions where tornado formation is more likely is the optical

324   thickening of low-level clouds through the activation of additional cloud droplets by the smoke

325   (Saide et al., 2015b). Thus, if this additional increase in NDROP is not substantial, it is expected

326   that environmental conditions would not change through this mechanism. 27 April 2011, which

327   is the other outbreak with strong smoke effects, also shows a factor of 2-3 increase on average

328   NDROP for vertical layers with cloud fractions over 0.2. Also, this outbreak presents a thick

329   layer of smoke on top of the clouds that is expected to exacerbate the smoke effects by

330   enhancing the capping inversion through soot absorption (Saide et al., 2015b), which in the

331   WRF-AAM configuration is included through the SSA of the mixture. The rest of the outbreaks

332 either did not present cloud fractions large enough nor sufficiently large changes to the cloud

333 droplet number concentration to produce regional effects on the environmental conditions.

334 Now, why does cloud droplet concentration increase due to smoke show large variability

335 between outbreaks? Considering only the layers with cloud fractions higher than 0.2, the

336 outbreaks with the largest NDROP increases (4 May 2003 and 27 April 2011) are those with the

337 largest increases in aerosol number concentrations due to smoke (Figure 7). For instance, in the

338 250-750m layer there is a 3-6 fold increase (on average) on aerosol number concentration for the

339 outbreaks with larger NDROP changes versus a ~2 fold increase for the rest of the outbreaks,

340 while for the 0.75-1.25 km layer the increases are 7-9 fold versus 3-4 fold. Thus, larger aerosol

341 number concentrations due to smoke in the cloudy layers can contribute to intensification of the

342 outbreaks (i.e., lower LCL, larger 1km shear and SRH), but it also depends on the overlying

343 background conditions. For instance, the 5 May 2007 outbreak presents larger aerosol number

344 concentrations at the cloud level compared to the 27 April 2011, but since the simulation without

345 fires shows very low aerosol number concentrations for 27 April 2011 the smoke effects are

346 amplified in this event. The vertical location of the smoke and its ability to reach the cloud layer

347 is also crucial, as for instance, the 28 April 2014 outbreak shows 5-6 fold enhancements in

348 aerosol number concentration due to smoke above the cloud layer but was not mixed downward

349 to provide large enhancements in NDROP. Other conditions affecting aerosol activation

350 including temperature and vertical wind velocities (Thompson and Eidhammer, 2014) can

351 change from outbreak to outbreak and could also play a role on the differences found.

352

353 3.4. Sensitivity simulations

354   We performed additional simulations to assess the effects of aerosol absorption and of changing

355   the initial smoke emissions. In the case of absorption, we modified the WRF-AAM code to use

356   single-scattering albedo (SSA) of a marine-type aerosol which absorbs radiation very weakly

357   (SSA of 0.99 at 70% relative humidity, versus 0.95 SSA of the rural type aerosol used in the base

358   simulations). The effect of absorption is then obtained by comparing simulations with smoke

359   emissions using the base configuration and the configuration just described. The other set of

360   sensitivity simulations performed used the FINN (Wiedinmyer et al., 2011) biomass burning

361   emissions as initial estimates and followed the same emission inversion scheme. All these

362   simulations were performed for three tornado outbreaks: 4 May 2003, 5 May 2007 and 15 April

363   2011. These outbreaks were chosen because they show a range of vertical smoke distributions

364   (mostly in the boundary layer and in the lower troposphere) and smoke effects (from large to

365   negligible effect size).

366   Figure 10 (top row) shows the effects of smoke on tornado parameters due to absorption. The

367   effect of absorption can vary from negligible to medium effect size depending on the outbreak

368   and the variable. The outbreak on 15 April 2011 presents a thick aerosol layer on top of the

369   shallow clouds going up to 4-5 km, while the smoke layer is mostly at cloud level or below on

370   the other two outbreaks (Figure 11, top-left panels). Previous studies have found that the location

371   of the smoke (or absorbing aerosol) with respect to clouds can be critical for the resulting effects,

372   with above cloud aerosol tending to increase cloudiness by enhancing the capping inversion,

373   while in-cloud aerosol can have the ability of burn-off clouds (Feingold et al., 2005; Johnson et

374   al., 2004). As seen in Figure 10, absorption makes LCL height shallower for the outbreak on 15

375   April 2011 while deeper for the other two. This is consistent with difference in the location of

376   smoke between simulations, as for 15 April 2011 cloud fraction tends to increase when the

377   smoke is absorbing while it is reduced for the other two outbreaks (Figure 11, bottom-left

378   panels). Note that for 5 May 2007 the overall effect of smoke on LCL is negligible (Figure 9,

379   top-left panel), thus absorption is counteracting the microphysical effects resulting in no apparent

380   effects. On the other hand, absorption tends to have a negligible effect or increase low-level wind

381   shear and SRH for all outbreaks. The increases are likely due to stabilization of the boundary

382   layer by aerosols on top of it. This is expected for the 15 April 2011 case due to the thick smoke

383   layer on top, and also occurs for the 4 May 2003 probably because this outbreak has the largest

384   smoke concentrations and the higher values are at the PBL height (Figure 7 and 8), so some of

385   this smoke is likely sitting right on top of the PBL generating these effects.

386   The smoke effects when using a different set of initial smoke emissions are shown on Figure 10

387   center-row panels and the vertical profiles can be found on Figure 11 right panels. The sensitivity

388   simulations are performed to assess smoke effects under different smoke loads. By comparing

389   Figure 11 and Figure 7 it can be seen that the resulting aerosol number concentration

390   distributions differ, with 5 May 2007 outbreak showing larger concentration enhancements due

391   to smoke in the sensitivity simulations and the 4 May 2003 and 15 April 2011 outbreaks showing

392   lower enhancements. The changes in smoke can have a variety of effects. For the 5 May 2007

393   and 15 April 2011 outbreaks the smoke effects remain similar in the sensitivity simulations

394   (Figure 10) compared to the base-line simulations (Figure 9), i.e. negligible smoke effects for the

395   5 May 2007 outbreak and small effect size for the 15 April 2011. On the other hand, smoke

396   effects change drastically for the 4 May 2003 outbreak, going from medium-large effect size for

397   the base-line simulation (Figure 9) to small effect size on the sensitivity simulation (Figure 10).

398   This is likely explained due to the lower aerosol loads in the sensitivity simulation which does

399   not generate the cloud fraction enhancement shown in the base-line case (Figure 11 vs. 7).

18

400   However, although there are differences in the magnitude of the smoke effects, the direction of

401   the change remains the same, i.e., smoke generates an increased likelihood of tornado formation

402   and intensity for both cases.

403

404   3.5. WRF-AAM vs WRF-Chem

405   In this section we compare WRF-AAM and WRF-Chem in terms of the AOD loads and smoke

406   effects.

407   The constrained emissions are influenced by the ability of the simplified aerosol species in the

408   AAM configuration to represent AOD. Figure 6 (top panels) shows a comparison between WRF-

409   AAM and WRF-Chem AOD for one of the outbreaks studied (27 April 2011). The similarity

410   between both simulations is remarkable given the differences in the aerosol model (a full

411   chemistry sectional scheme with 8 size bins versus two aerosol species), the optical properties

412   parameterization (a Mie code including a core-shell treatment versus a table look-up approach)

413   and the cloud physics parameterizations (Morrison (Yang et al., 2011 and references therein)

414   versus TE2014 microphysics). Some of the differences between the simulations are due to the

415   way each treats the hygroscopic growth of smoke. In the case of WRF-Chem configured with

416   MOSAIC, aerosol hygroscopic growth is done through the electrolytes in the aerosol mixture,

417   and as organic carbon and black carbon are not considered as electrolytes in this model

418   configuration, there is little hygroscopic growth for smoke. For the AAM configuration the

419   opposite happens, as organic carbon emissions are lumped into the hygroscopic aerosol

420   (hygroscopicity parameter equals to 0.4) and thus undergo significant water uptake. There are

421   large differences in the northwest of the Gulf of Mexico between WRF-AAM and WRF-Chem

422 (Figure 6), which are due to the differences in hygroscopic growth as some model layers show

423 large values of relative humidity (RH) in this region at this time. The localized spikes in the

424 WRF-AAM AOD that are not seen in the WRF-Chem AOD are also due to hygroscopic growth.

425 Thus, we expect to obtain slightly lower emission correction factors when performing the

426 inversion with the AAM than with WRF-Chem due to the larger AOD obtained because of the

427 hygroscopic growth of smoke.

428 As mentioned previously, non-negligible smoke effects are found for the 27 April 2011 outbreak

429 when using the AAM configuration. Saide et al. (2015b), using WRF-Chem, reported 100-200 m

430 lower LCL, ~2 m/s higher low-level wind shear and ~50 m^2/s^2 higher SRH as a result of smoke

431 interactions with clouds and radiation, which is in the same direction and of similar values to

432 what is found with WRF-AAM for this event (Figure 9). This agreement is again noteworthy

433 given the complex aerosol-cloud-radiation interactions that occur in this system and the way they

434 are parameterized differently in each model configuration (e.g., aerosol optical properties,

435 aerosol size distribution, cloud microphysics, aerosol activation, etc.).

436 We performed WRF-Chem simulations for the three outbreaks studied in the sensitivity

437 simulations (Section 3.4) to further assess similarities and differences with respect to the WRF-

438 AAM configuration. Figures 7 and 12 (top panels) show that aerosol number concentrations for

439 simulations with and without fire emissions are consistent within the two systems. Note that the

440 WRF-Chem concentrations are shown only for the accumulation mode and thus aerosol number

441 concentrations are much lower compared to WRF-AAM. Although in WRF-Chem total aerosol

442 number is dominated by ultra-fine particles from new particle formation, these particles tend to

443 contribute less to CCN than accumulation mode particles and thus cloud droplet numbers are

444   higher in simulations with smoke (Figure 12, center-row panels), which is consistent with WRF-

445   AAM simulations.

446   As seen in Figure 10 (bottom panels), smoke intensifies tornado parameters for all cases when

447   using WRF-Chem with effect size on the small to medium range. This is generally consistent

448   with the WRF-AAM simulations, as with this system the 4 May 2003 and 15 April 2011

449   outbreaks show intensification with small to large effect size, while 5 May 2007 shows

450   negligible effects (Figure 9 top panels). There could be multiple reasons for these discrepancies.

451   For instance, for the 4 May 2003 outbreak the enhancement in cloud droplet number

452   concentration due to smoke for WRF-AAM (Figure 7) is larger than for WRF-Chem (Figure 12)

453   which contributes to a larger effect size in tornado parameters for WRF-AAM for this outbreak.

454   The higher cloud droplet number concentration in WRF-AAM could be due to the differences

455   between the aerosol activation parameterizations in WRF-Chem and WRF-AAM as droplet

456   nucleation could get saturated at different aerosol loadings. Aerosol optical properties could also

457   be producing some of these differences, as the smoke is more absorbing on WRF-Chem (SSA of

458   0.93-0.94 on the region of the 4 May 2003 outbreak) than on WRF-AAM (SSA over 0.96 for RH

459   over 80%), thus the burn-off of clouds due to absorption found in section 3.4 for the 4 May 2003

460   outbreak could be occurring more efficiently in WRF-Chem and thus preventing the large

461   enhancement in cloud fraction seen in WRF-AAM. For the 5 May 2007 outbreak the aerosol

462   concentrations are maximum at the surface, which generates a different response in WRF-AAM

463   and WRF-Chem, with WRF-Chem increasing cloud fractions due to smoke at the lower levels

464   (below 750m) and thus intensifying the tornado parameters where in WRF-AAM only negligible

465   changes are found.

466   **4. Conclusions**

467   In this study we used the WRF modeling system configured with an aerosol-aware microphysics

468   (AAM) parameterization to study impacts of smoke from Central America on multiple tornado

469   outbreaks in the US happening during the fire season. To do so, we included emission processes

470   into the WRF-AAM by using WRF-Chem routines that add primary aerosol emissions to the

471   model. Also, we constrained biomass burning emissions for each outbreak studied using satellite-

472   derived AOD and an inverse modeling algorithm. We found a general underestimation of the

473   prior emissions but with large spatial and temporal variations. This is important as studies not

474   using an observational constraint are likely to underestimate the smoke effects, and this cannot

475   be fixed by just applying a global correction factor to emissions.

476   Using the WRF aerosol-aware-microphysics configuration, we found smoke present in the

477   boundary layer of all outbreaks studied with some cases presenting a thick layer of smoke aloft.

478   Across the various cases studied, we also found a large spread of the smoke effects on

479   environmental conditions, going from negligible impacts to intensifications due to smoke (i.e., a

480   reduction of LCL and increase in low level wind shear and SRH) which are in the range of

481   differences found in the sounding climatology within adjacent supercell classes (Thompson et

482   al., 2003). Smoke effects on environmental conditions were considerable when there was a

483   distinct layer of low level clouds (cloud fraction >0.2) and the smoke largely increased aerosol

484   number concentration over background values (3-9 fold), producing large cloud droplet

485   concentration increases (2-3 fold). We found that the presence of a thick layer of smoke above

486   the low-level clouds can contribute to the intensifications of tornado parameters. However, when

487   this layer is not present and smoke concentration at cloud level is large, aerosol absorption can

488   produce cloud-burn off which can deepen the LCL heights, counteracting the microphysical

489   effects. Sensitivity simulations also showed that when changing smoke emissions the smoke

490   effects on tornado parameters were consistent but the magnitudes could vary with the emissions

491   amount.

492   In this study we only analyzed the effects of biomass burning smoke on environmental

493   conditions that lead to a higher likelihood of tornado formation and intensity. Other studies have

494   proposed alternative mechanisms such as convection invigoration to link smoke with tornadoes

495   (Wang et al., 2009), or suggested that tornado occurrence have a weekly cycle due to

496   anthropogenic activities (Rosenfeld and Bell, 2011). Recent evidence has shown that fires also

497   present a weekly cycle (Earl et al., 2015). Given our finding that smoke was present for all

498   outbreaks studied, and that can be a major contributor to aerosol number concentrations in all the

499   cases, the role of fires in these other mechanisms needs to be included in future work studying

500   tornadoes during the fire season. Also, given that the Gulf of Mexico is a common source of

501   moisture for severe thunderstorms (Brooks et al., 2003), we expect smoke to be transported

502   along with moisture during the burning season, thus future work should assess the effects of

503   smoke for severe weather other than tornadoes (e.g., large hail and damaging winds).

504   Finally, we also compared WRF configured with aerosol-aware-microphysics to WRF-Chem.

505   Although these model configurations use different parameterizations of aerosol optical

506   properties, aerosol size, cloud microphysics and cloud droplet nucleation, we found their results

507   are generally consistent. In particular, they show comparable AODs over the region affected with

508   smoke, similar smoke transport patterns to the outbreak region and consistent smoke effects on

509   environmental conditions which can lead to intensification of the outbreak. Thus, the aerosol-

510   cloud-radiation interactions included in WRF-AAM are generally in agreement with more

511   complex models and given the current restrictions on computing power dedicated to these

512   interactions they represent a good choice for the moment. This is encouraging as the AAM is

513   planned to become one of National Centers for Environmental Prediction (NCEP) operational

514   configurations (Rapid Refresh and High-Resolution Rapid Refresh forecasts). The method to

515   constrain emissions coupled to the WRF-AAM is also computationally efficient as it only

516   requires two simulations (no adjoint, no ensembles), thus it could be implemented in near-real

517   time applications to constrain highly uncertain emissions such as those from fires and wind-

518   blown dust.

Acknowledgments

References

530   Abdul-Razzak, H. and Ghan, S. J.: A parameterization of aerosol activation 3. Sectional
531   representation, J. Geophys. Res., 107, 4026, 2002.

532   Andreae, M. O. and Rosenfeld, D.: Aerosol–cloud–precipitation interactions. Part 1. The nature
533   and sources of cloud-active aerosols, Earth-Science Reviews, 89, 13-41, 2008.

534   Barlage, M., Chen, F., Tewari, M., Ikeda, K., Gochis, D., Dudhia, J., Rasmussen, R., Livneh, B.,
535   Ek, M., and Mitchell, K.: Noah land surface model modifications to improve snowpack
536   prediction in the Colorado Rocky Mountains, Journal of Geophysical Research: Atmospheres,
537   115, D22101, 2010.

538   Barrett, B. S. and Gensini, V. A.: Variability of central United States April–May tornado day
539   likelihood by phase of the Madden-Julian Oscillation, Geophysical Research Letters, 40, 2790-
540   2795, 2013.

541   Blunden, J. and Arndt, D. S.: State of the Climate in 2011, Bulletin of the American
542   Meteorological Society, 93, S1-S282, 2012.

543 Blunden, J. and Arndt, D. S.: State of the Climate in 2013, Bulletin of the American
544 Meteorological Society, 95, S1-S279, 2014.

545 Blunden, J. and Arndt, D. S.: State of the Climate in 2014, Bulletin of the American
546 Meteorological Society, 96, ES1-ES32, 2015.

547 Bond, T. C., Streets, D. G., Yarber, K. F., Nelson, S. M., Woo, J.-H., and Klimont, Z.: A
548 technology-based global inventory of black and organic carbon emissions from combustion,
549 Journal of Geophysical Research: Atmospheres, 109, D14203, 2004.

550 Boucher, O., Randall, D., Artaxo, P., Bretherton, C., Feingold, G., Forster, P., Kerminen, V.-M.,
551 Kondo, Y., Liao, H., Lohmann, U., Rasch, P., Satheesh, S. K., Sherwood, S., Stevens, B., and
552 Zhang, X. Y.: Clouds and Aerosols. In: Climate Change 2013: The Physical Science Basis.
553 Contribution of Working Group I to the Fifth Assessment Report of the Intergovernmental 25
554 Panel on Climate Change, edited by: Stocker, T. F., Qin, D., Plattner, G.-K., Tignor, M., Allen,
555 S. K., Boschung, J., Nauels, A., Xia, Y., Bex, V., and Midgley, P. M, Cambridge University
556 Press, Cambridge, United Kingdom and New York, NY, USA, 2013.

557 Brooks, H. E.: Severe thunderstorms and climate change, Atmospheric Research, 123, 129-138,
558 2013.

559 Brooks, H. E. and Doswell, C. A.: Deaths in the 3 May 1999 Oklahoma City Tornado from a
560 Historical Perspective, Weather and Forecasting, 17, 354-361, 2002.

561 Brooks, H. E., Lee, J. W., and Craven, J. P.: The spatial distribution of severe thunderstorm and
562 tornado environments from global reanalysis data, Atmospheric Research, 67–68, 73-94, 2003.

563 Darmenov, A. and da Silva, A. M.: The Quick Fire Emissions Dataset (QFED) - Documentation
564 of versions 2.1, 2.2 and 2.4, NASA/TM–2015–104606, Vol. 38., (
565 http://gmao.gsfc.nasa.gov/pubs/tm/), 183 pp, 2015.

566 Diffenbaugh, N. S., Scherer, M., and Trapp, R. J.: Robust increases in severe thunderstorm
567 environments in response to greenhouse forcing, Proceedings of the National Academy of
568 Sciences, 110, 16361-16366, 2013.

569 Earl, N., Simmonds, I., and Tapper, N.: Weekly cycles of global fires—Associations with
570 religion, wealth and culture, and insights into anthropogenic influences on global climate,
571 Geophysical Research Letters, 42, 2015GL066383, 2015.

572 Eidhammer, T., Barth, M. C., Petters, M. D., Wiedinmyer, C., and Prenni, A. J.: Aerosol
573 microphysical impact on summertime convective precipitation in the Rocky Mountain region,
574 Journal of Geophysical Research: Atmospheres, 2014JD021883, 2014.

575 Emmons, L. K., Walters, S., Hess, P. G., Lamarque, J. F., Pfister, G. G., Fillmore, D., Granier,
576 C., Guenther, A., Kinnison, D., Laepple, T., Orlando, J., Tie, X., Tyndall, G., Wiedinmyer, C.,
577 Baughcum, S. L., and Kloster, S.: Description and evaluation of the Model for Ozone and
578 Related chemical Tracers, version 4 (MOZART-4), Geosci. Model Dev., 3, 43-67, 2010.

579 Feingold, G., Jiang, H., and Harrington, J. Y.: On smoke suppression of clouds in Amazonia,
580 Geophysical research letters, 32, L02804, 2005.

581 Freitas, S. R., Longo, K. M., Alonso, M. F., Pirre, M., Marecal, V., Grell, G., Stockler, R., Mello,
582 R. F., and Sánchez Gácita, M.: PREP-CHEM-SRC – 1.0: a preprocessor of trace gas and aerosol
583 emission fields for regional and global atmospheric chemistry models, Geosci. Model Dev., 4,
584 419-433, 2011.

585 GMAO: http://gmao.gsfc.nasa.gov/forecasts, 2014.

586 Gong, S., Barrie, L., and Blanchet, J.-P.: Modeling sea-salt aerosols in the atmosphere 1. Model
587 development, Journal of Geophysical Research, 102, 3805-3818, 1997.

588 Grell, G., Freitas, S. R., Stuefer, M., and Fast, J.: Inclusion of biomass burning in WRF-Chem:
589 impact of wildfires on weather forecasts, Atmos. Chem. Phys., 11, 5289-5303, 2011.

590 Grell, G. A. and Freitas, S. R.: A scale and aerosol aware stochastic convective parameterization
591 for weather and air quality modeling, Atmos. Chem. Phys. Discuss., 13, 23845-23893, 2013.

592 Hamill, T. M., Schneider, R. S., Brooks, H. E., Forbes, G. S., Bluestein, H. B., Steinberg, M.,
593 Meléndez, D., and Dole, R. M.: The May 2003 Extended Tornado Outbreak, Bulletin of the
594 American Meteorological Society, 86, 531-542, 2005.

595 Holben, B., Tanré, D., Smirnov, A., Eck, T., Slutsker, I., Abuhassan, N., Newcomb, W., Schafer,
596 J., Chatenet, B., and Lavenu, F.: An emerging ground-based aerosol climatology: Aerosol optical
597 depth from AERONET, Journal of Geophysical Research, 106, 12067-12012,12097, 2001.

598 Iacono, M. J., Delamere, J. S., Mlawer, E. J., Shephard, M. W., Clough, S. A., and Collins, W.
599 D.: Radiative forcing by long-lived greenhouse gases: Calculations with the AER radiative
600 transfer models, Journal of Geophysical Research: Atmospheres, 113, D13103, 2008.

601 Iacono, M. J., Mlawer, E. J., Clough, S. A., and Morcrette, J.-J.: Impact of an improved
602 longwave radiation model, RRTM, on the energy budget and thermodynamic properties of the
603 NCAR community climate model, CCM3, Journal of Geophysical Research: Atmospheres, 105,
604 14873-14890, 2000.

605 Jacobson, M. Z.: Effects of biomass burning on climate, accounting for heat and moisture fluxes,
606 black and brown carbon, and cloud absorption effects, Journal of Geophysical Research:
607 Atmospheres, 2014JD021861, 2014.

608 Janjić, Z. I.: Nonsingular implementation of the Mellor–Yamada level 2.5 scheme in the NCEP
609 Meso model, NCEP office note, 437, 61, 2002.

610 Johnson, B. T., Shine, K. P., and Forster, P. M.: The semi-direct aerosol effect: Impact of
611 absorbing aerosols on marine stratocumulus, Quarterly Journal of the Royal Meteorological
612 Society, 130, 1407-1422, 2004.

Kaiser, J. W., Heil, A., Andreae, M. O., Benedetti, A., Chubarova, N., Jones, L., Morcrette, J. J., Razinger, M., Schultz, M. G., Suttie, M., and van der Werf, G. R.: Biomass burning emissions estimated with a global fire assimilation system based on observed fire radiative power, Biogeosciences, 9, 527-554, 2012.

Knupp, K. R., Murphy, T. A., Coleman, T. A., Wade, R. A., Mullins, S. A., Schultz, C. J., Schultz, E. V., Carey, L., Sherrer, A., McCaul, E. W., Carcione, B., Latimer, S., Kula, A., Laws, K., Marsh, P. T., and Klockow, K.: Meteorological Overview of the Devastating 27 April 2011 Tornado Outbreak, Bulletin of the American Meteorological Society, 2013.

Kolusu, S. R., Marsham, J. H., Mulcahy, J., Johnson, B., Dunning, C., Bush, M., and Spracklen, D. V.: Impacts of Amazonia biomass burning aerosols assessed from short-range weather forecasts, Atmos. Chem. Phys., 15, 12251-12266, 2015.

Lebo, Z. J. and Morrison, H.: A Novel Scheme for Parameterizing Aerosol Processing in Warm Clouds, Journal of the Atmospheric Sciences, 70, 3576-3598, 2013.

Levinson, D. H. and Lawrimore, J. H.: State of the Climate in 2007, Bulletin of the American Meteorological Society, 89, S1-S179, 2008.

Levinson, D. H. and Waple, A. M.: State of the Climate in 2003, Bulletin of the American Meteorological Society, 85, 881-881, 2004.

Markowski, P. M. and Richardson, Y. P.: Tornadogenesis: Our current understanding, forecasting considerations, and questions to guide future research, Atmospheric Research, 93, 3-10, 2009.

Mena-Carrasco, M., Carmichael, G. R., Campbell, J. E., Zimmerman, D., Tang, Y., Adhikary, B., D'Allura, A., Molina, L. T., Zavala, M., García, A., Flocke, F., Campos, T., Weinheimer, A. J., Shetter, R., Apel, E., Montzka, D. D., Knapp, D. J., and Zheng, W.: Assessing the regional impacts of Mexico City emissions on air quality and chemistry, Atmos. Chem. Phys., 9, 3731-3743, 2009.

NCEP: NCEP FNL Operational Model Global Tropospheric Analyses, continuing from July 1999. Research Data Archive at the National Center for Atmospheric Research, Computational and Information Systems Laboratory, Boulder, CO, 2000.

Peterson, T. C. and Baringer, M. O.: State of the Climate in 2008, Bulletin of the American Meteorological Society, 90, S1-S196, 2009.

Potter, S.: Fine-Tuning Fujita: After 35 years, a new scale for rating tornadoes takes effect, Weatherwise, 60, 64-71, 2007.

Rasmussen, E. N. and Blanchard, D. O.: A Baseline Climatology of Sounding-Derived Supercell and Tornado Forecast Parameters, Weather and Forecasting, 13, 1148-1164, 1998.

Reid, J. S., Prins, E. M., Westphal, D. L., Schmidt, C. C., Richardson, K. A., Christopher, S. A., Eck, T. F., Reid, E. A., Curtis, C. A., and Hoffman, J. P.: Real-time monitoring of South

American smoke particle emissions and transport using a coupled remote sensing/box-model approach, Geophysical Research Letters, 31, L06107, 2004.

Rosenfeld, D. and Bell, T. L.: Why do tornados and hailstorms rest on weekends?, Journal of Geophysical Research (Atmospheres), 116, 20211, 2011.

Ruiz-Arias, J. A., Dudhia, J., and Gueymard, C. A.: A simple parameterization of the short-wave aerosol optical properties for surface direct and diffuse irradiances assessment in a numerical weather model, Geosci. Model Dev., 7, 1159-1174, 2014.

Saide, P. E., Carmichael, G. R., Liu, Z., Schwartz, C. S., Lin, H. C., da Silva, A. M., and Hyer, E.: Aerosol optical depth assimilation for a size-resolved sectional model: impacts of observationally constrained, multi-wavelength and fine mode retrievals on regional scale analyses and forecasts, Atmos. Chem. Phys., 13, 10425-10444, 2013.

Saide, P. E., Peterson, D., da Silva, A., Anderson, B., Ziemba, L. D., Diskin, G., Sachse, G., Hair, J., Butler, C., Fenn, M., Jimenez, J. L., Campuzano-Jost, P., Perring, A. E., Schwarz, J. P., Markovic, M. Z., Russell, P., Redemann, J., Shinozuka, Y., Streets, D. G., Yan, F., Dibb, J., Yokelson, R., Toon, O. B., Hyer, E., and Carmichael, G. R.: Revealing important nocturnal and day-to-day variations in fire smoke emissions through a multiplatform inversion, Geophysical research letters, 2015GL063737, 2015a.

Saide, P. E., Spak, S. N., Pierce, R. B., Otkin, J. A., Schaack, T. K., Heidinger, A. K., da Silva, A. M., Kacenelenbogen, M., Redemann, J., and Carmichael, G. R.: Central American biomass burning smoke can increase tornado severity in the U.S, Geophysical research letters, 42, 2014GL062826, 2015b.

Sullivan, G. M. and Feinn, R.: Using Effect Size—or Why the P Value Is Not Enough, Journal of Graduate Medical Education, 4, 279-282, 2012.

Thompson, G. and Eidhammer, T.: A Study of Aerosol Impacts on Clouds and Precipitation Development in a Large Winter Cyclone, Journal of the atmospheric sciences, 71, 3636-3658, 2014.

Thompson, R. L., Edwards, R., and Hart, J. A.: Evaluation and interpretation of the Supercell Composite and the Significant Tornado Parameters at the Storm Prediction Centre. Preprints, 21st Conf. on Severe Local Storms, San Antonio, TX, Amer. Meteor. Soc., J11-J14, 2002.

Thompson, R. L., Edwards, R., Hart, J. A., Elmore, K. L., and Markowski, P.: Close Proximity Soundings within Supercell Environments Obtained from the Rapid Update Cycle, Weather and Forecasting, 18, 1243-1261, 2003.

Wang, J., Christopher, S. A., Nair, U. S., Reid, J. S., Prins, E. M., Szykman, J., and Hand, J. L.: Mesoscale modeling of Central American smoke transport to the United States: 1. "Top-down" assessment of emission strength and diurnal variation impacts, Journal of Geophysical Research: Atmospheres, 111, D05S17, 2006.

685   Wang, J., van den Heever, S., and Reid, J.: A conceptual model for the link between Central
686   American biomass burning aerosols and severe weather over the south central United States,
687   Environmental Research Letters, 4, 015003, 2009.

688   Wiedinmyer, C., Akagi, S. K., Yokelson, R. J., Emmons, L. K., Al-Saadi, J. A., Orlando, J. J.,
689   and Soja, A. J.: The Fire INventory from NCAR (FINN): a high resolution global model to
690   estimate the emissions from open burning, Geosci. Model Dev., 4, 625-641, 2011.

691   Wolf, M. E., Fields, P. G., Manne, G. K., Villegas, M. T. L., Bravo, V. G., Gómez, R. I.,
692   Periférico, C., Cuicuilco, C. I., and Coyoacán, D.: Developing Mexico National Emissions
693   Inventory Projections for the Future Years of 2008, 2012, and 2030, 2009.

694   Yang, Q., W. I. Gustafson, J., Fast, J. D., Wang, H., Easter, R. C., Morrison, H., Lee, Y. N.,
695   Chapman, E. G., Spak, S. N., and Mena-Carrasco, M. A.: Assessing regional scale predictions of
696   aerosols, marine stratocumulus, and their interactions during VOCALS-REx using WRF-Chem,
697   Atmospheric Chemistry and Physics, 11, 11951-11975, 2011.

698   Zaveri, R. A., Easter, R. C., Fast, J. D., and Peters, L. K.: Model for simulating aerosol
699   interactions and chemistry (MOSAIC), J. Geophys. Res, 113, D13204, 2008.

700   Zaveri, R. A. and Peters, L. K.: A new lumped structure photochemical mechanism for large-
701   scale applications, Journal of Geophysical Research, 104, 30387-30330,30415, 1999.

702   Zhang, F., Wang, J., Ichoku, C., Hyer, E. J., Yang, Z., Ge, C., Su, S., Zhang, X., Kondragunta,
703   S., and Kaiser, J. W.: Sensitivity of mesoscale modeling of smoke direct radiative effect to the
704   emission inventory: a case study in northern sub-Saharan African region, Environmental
705   Research Letters, 9, 075002, 2014.

706   Zhao, C., Liu, X., Leung, L. R., Johnson, B., McFarlane, S. A., Gustafson Jr, W. I., Fast, J. D.,
707   and Easter, R.: The spatial distribution of mineral dust and its shortwave radiative forcing over
708   North Africa: modeling sensitivities to dust emissions and aerosol size treatments, Atmos. Chem.
709   Phys., 10, 8821-8838, 2010.

710 **Figures**
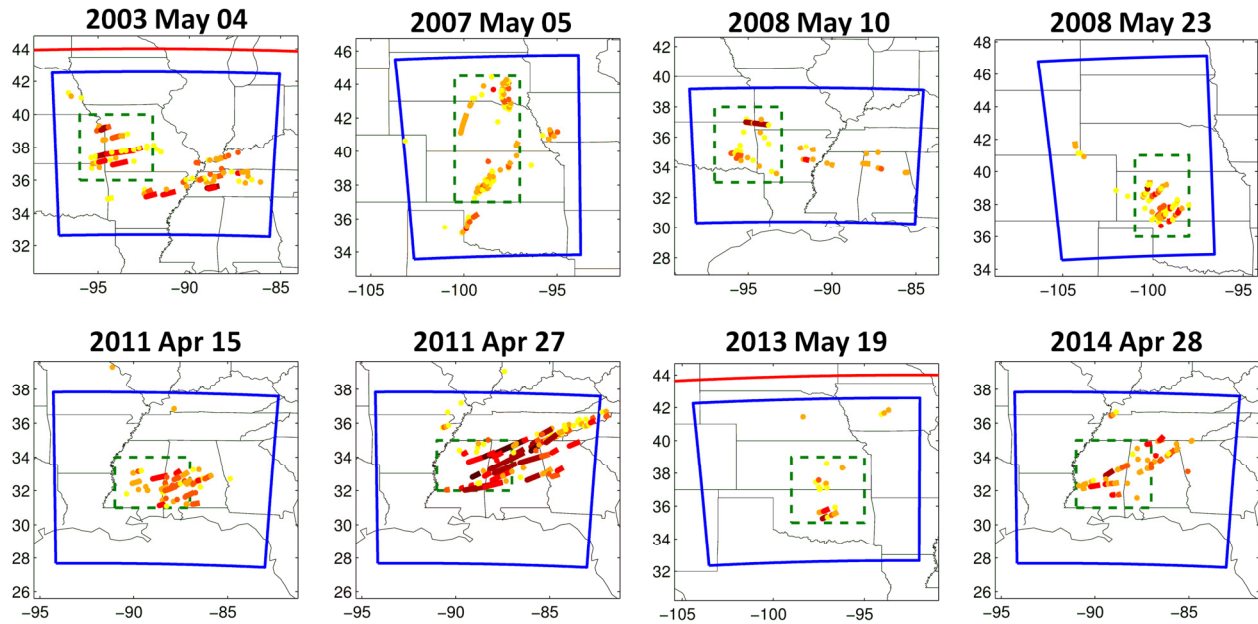
Figure 1. Tornado tracks of the outbreaks studied color-coded by Enhanced Fujita (EF) Scale
(Potter, 2007), with darker colors representing higher magnitude. Blue solid lines represent the
inner domain specified for each simulation. Boundaries of the outer domain are in red solid lines
when included in the regions shown (see full outer domains in Figure 2). Green segmented lines
show the region where statistics are computed which corresponds to the area where the earlier
tornadoes occur.

2003 May 04 **2007 May 05 20Z** **2008 May 10 21Z** **2008 May 23 22Z**

2011 Apr 15 20Z **2011 Apr 27 18Z** **2013 May 19 20Z** **2014 Apr 28 19Z**

718
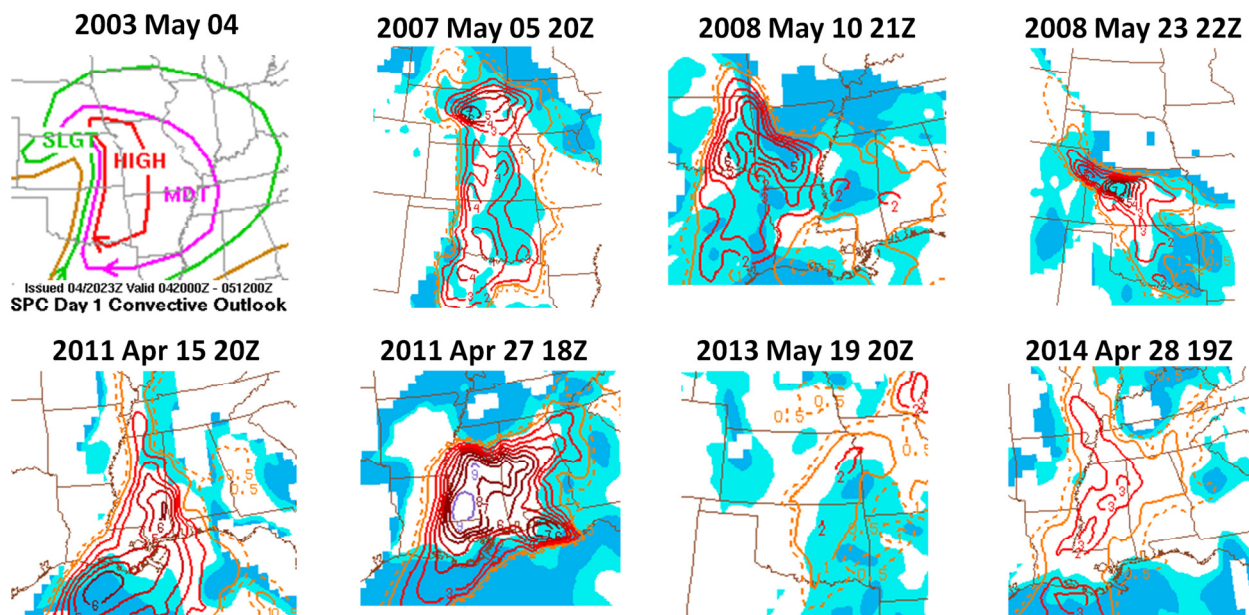
719 Figure 2. Environmental conditions for the outbreaks studied as provided by the SPC. While the

720 day 1 convective outlook valid at 23 UTC is shown for 2003 May 4, the fixed-layer Significant

721 Tornado Parameter (STP, in contours) and the Convective Inhibition (CIN, shaded at 25 and 100

722 J/kg) obtained from the houlrly Mesoscale Analysis are shown for the rest of the outbreaks.

723
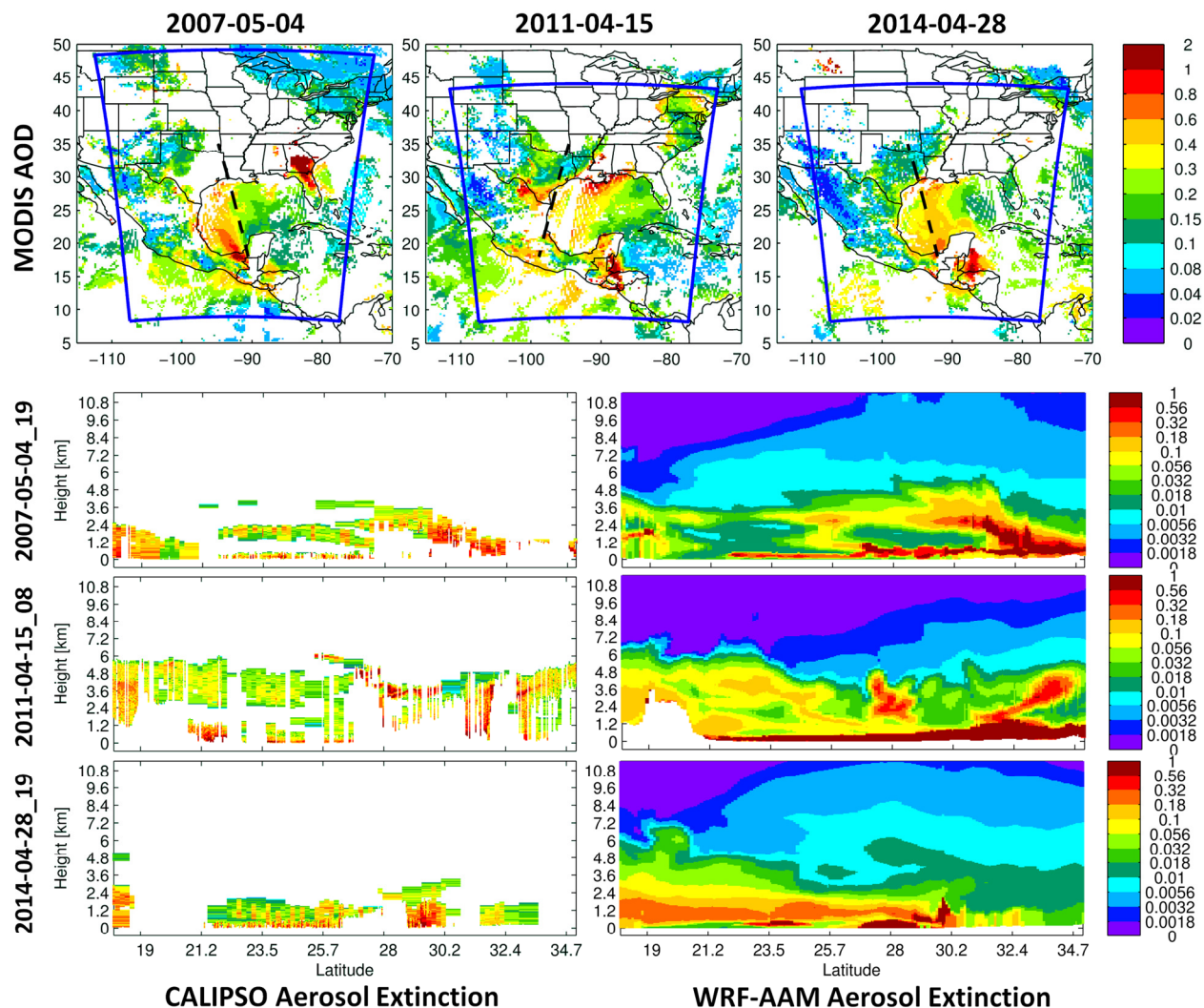
Figure 3. Top panels: Observed AOD maps on the day or the day before of three outbreaks studied (5 May 2007 on the left, 15 April 2011 on the middle, and 28 April 2014 on the right) by combining Terra and Aqua overpasses. The solid blue line represents the outer domains used for these outbreaks. Bottom panels: Observed and modeled (Fire ON + inversion) extinction (1/km) curtains. The CALIPSO tracks corresponding to these observations are shown as dashed black lines on the top panels.

732
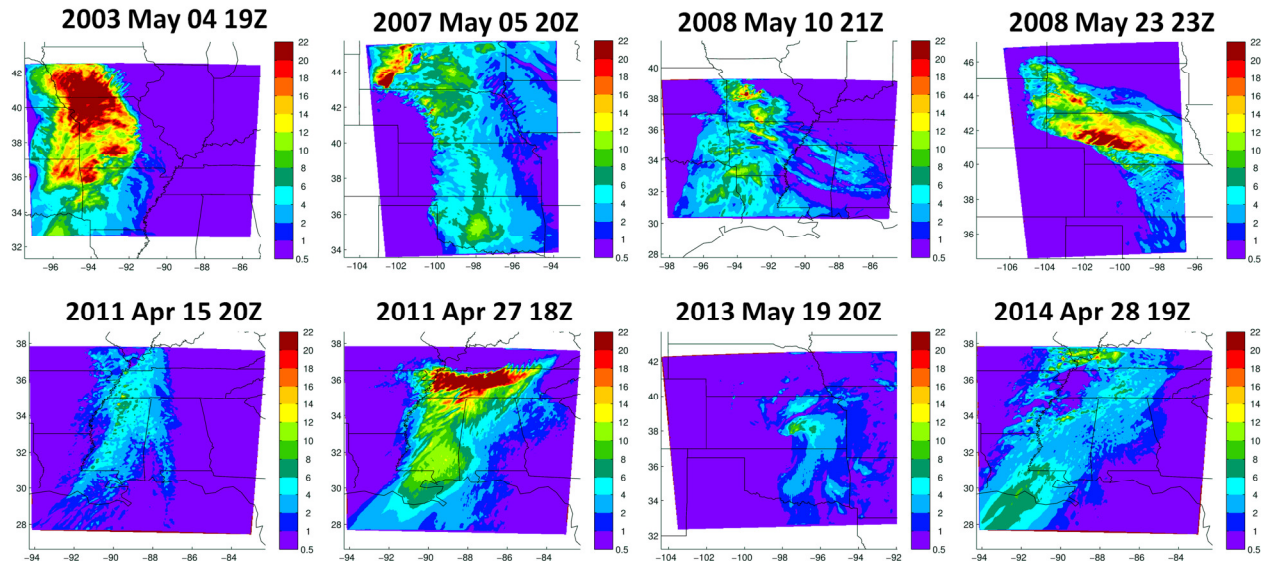
Figure 4. Significant Tornado Parameter (STP) at the beginning of each outbreak studied as

modeled by the WRF-AAM configuration when using the contrained fire emissions.
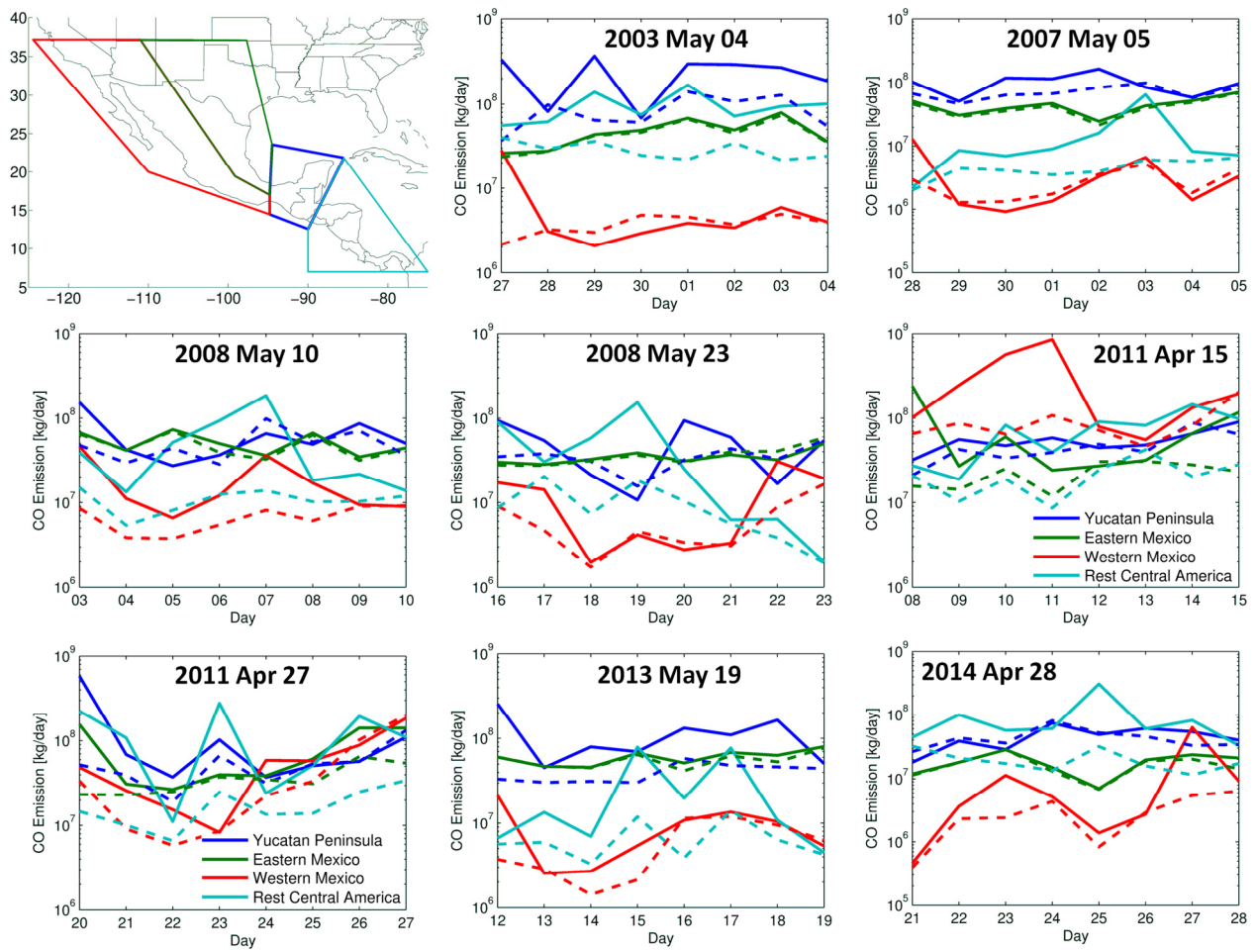
Figure 5. Top-left panel: Regions used to tag fire emissions tracers (see Section 2.3). Rest of the panels: Constrained (solid lines) and first-guess (segmented lines) emissions by day on each region and for each outbreak (indicated at the top of each panel).

739
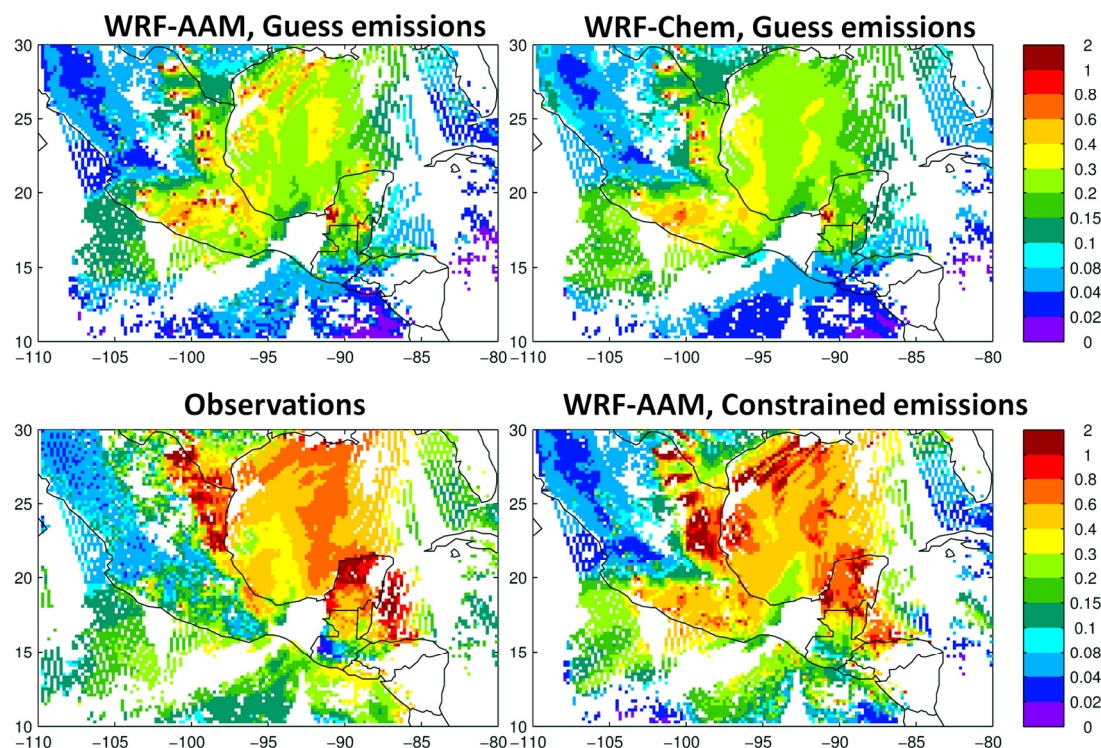
Figure 6. AOD maps for the observations and three model simulations on 27 April 2011 by
combining Terra and Aqua overpasses. Cloudy grid-cells are not considered when computing
model AOD.
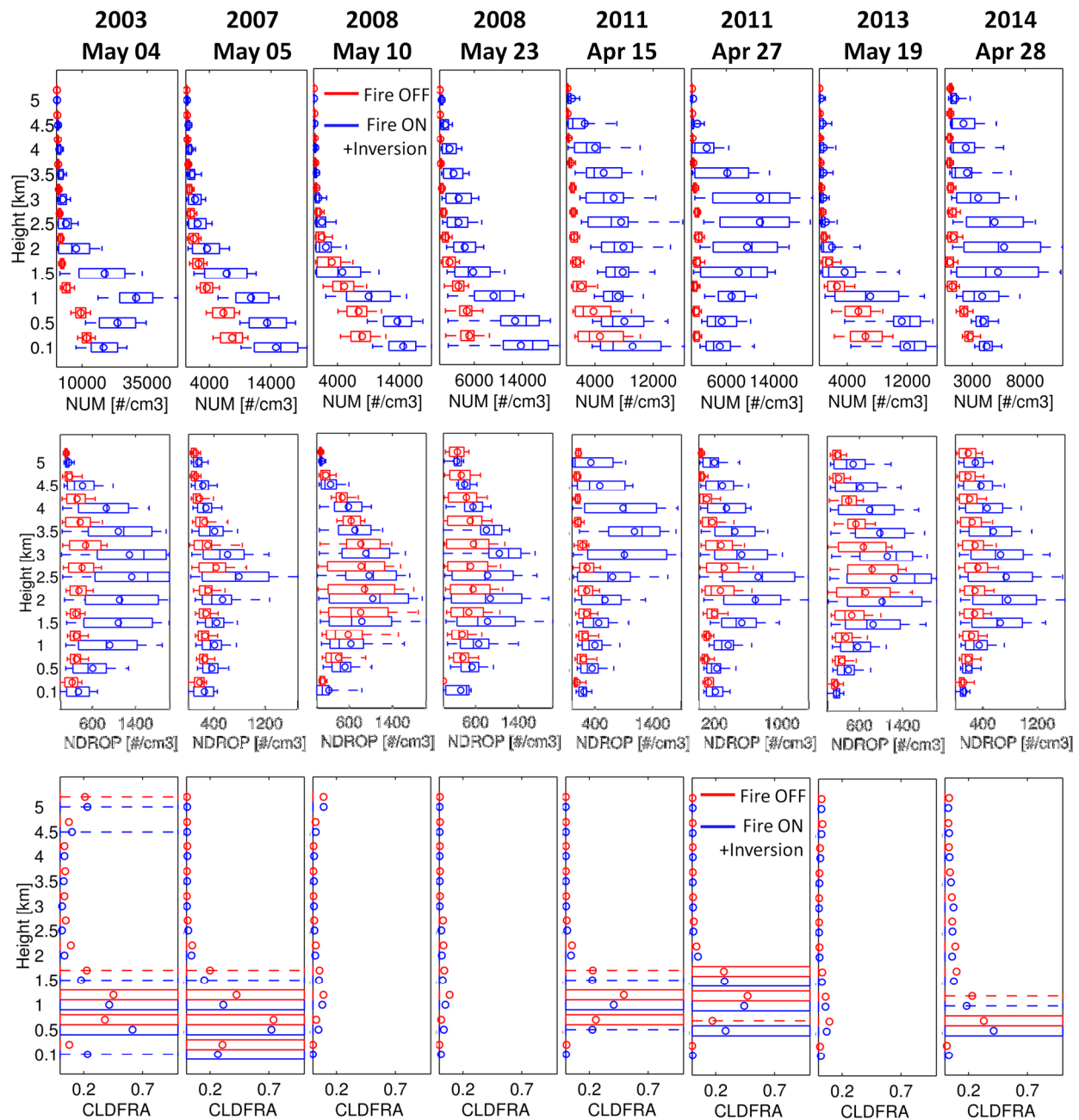
Figure 7. Vertical distributions of modeled (WRF-AAM) aerosol number concentration (NUM),

cloud droplet concentration (NDROP), and cloud fraction (CLDFRA) for the cases studied

turning on and off biomass burning emissions. The distributions are shown as box plots, with

center solid lines indicate the median, circles representing the mean, boxes indicating upper and

lower quartiles, and whiskers showing the upper and lower deciles. Statistics are computed for

749   the regions shown in Figure 1 and one hour before the outbreak starts. Note that cloud fraction is

750   either 0 or 1 in this WRF configuration, thus the boxes and whiskers either use the whole 0-1

751   interval or collapse to zero for low cloud fractions. X-axes start at a value of 0 for all panels.
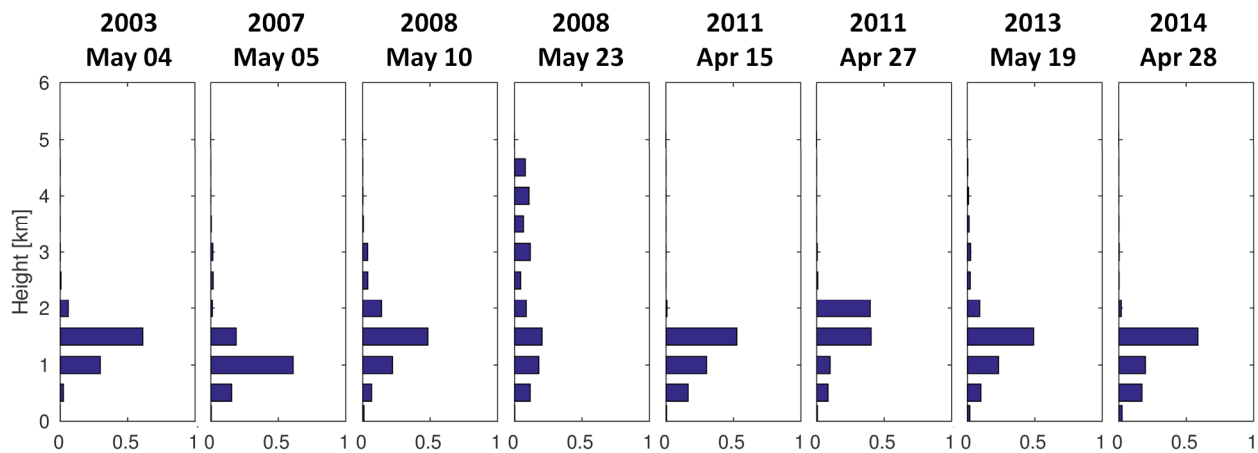
753   Figure 8. Normalized histograms of boundary layer height for the same regions, height
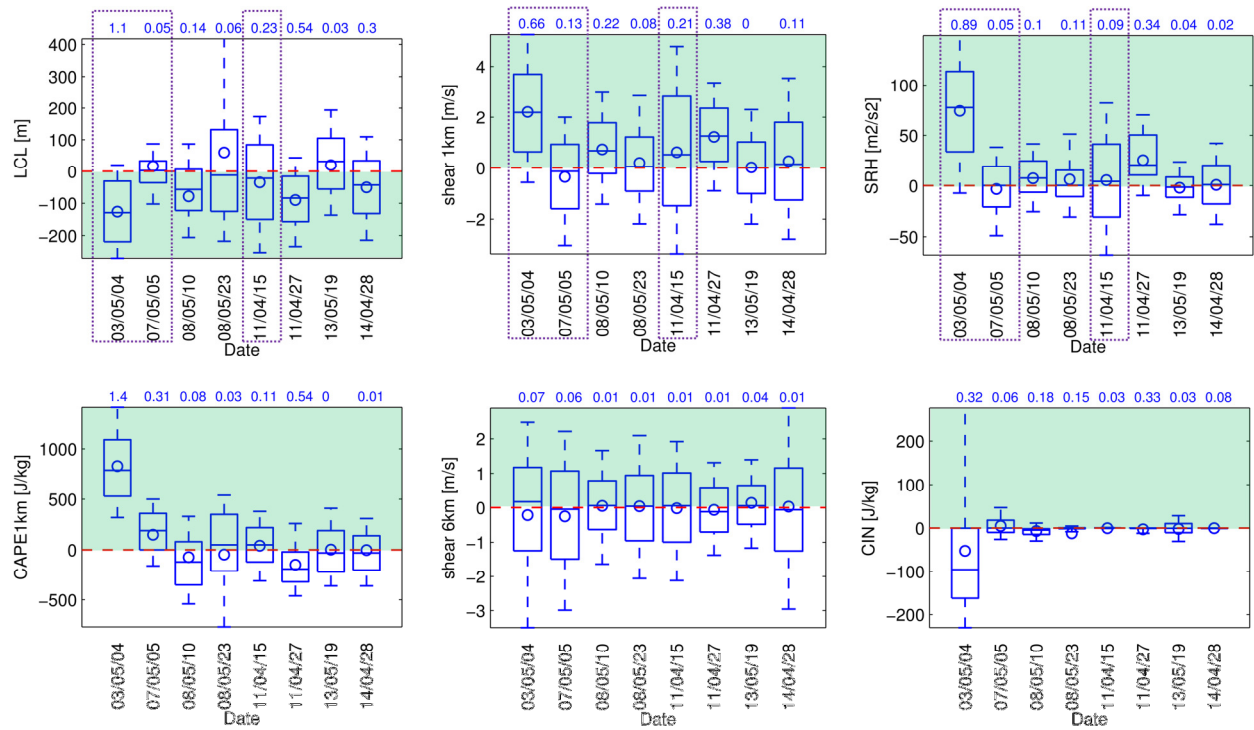
754   categories and outbreaks as in Figure 7.

755

Figure 9. Statistics (as in Figure 7) of the differences between WRF-AAM simulations with and without fire emissions. The standardized difference (effect size) between both simulations is shown on top of each panel. The dashed red lines indicate the zero difference line, while the green area denotes the region where the smoke increases the likelihood of tornado occurrence and intensity (decrease in LCL, increase in 1km shear and SRH) and a higher chance of convection (increased CAPE, 6km shear and CIN). The dotted purple rectangles highlight the sensitivity cases and variables studied in the next figures. Note that CIN is a negative quantity. Dates are in YY/MM/DD format.

767
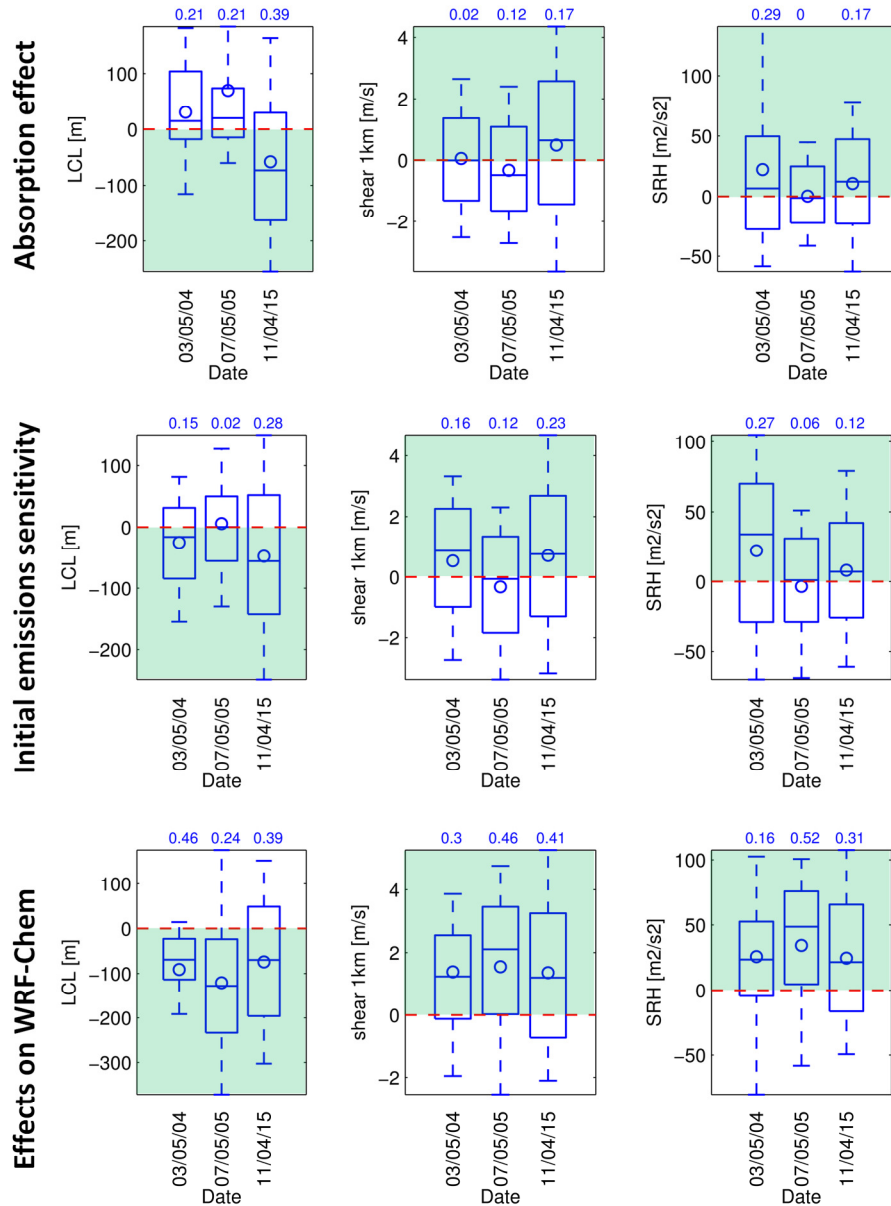
Figure 10. As Figure 9 but for the sensitivity cases and WRF-Chem simulations. Note that

sensitivity runs for testing the effect of absorption compare two simulations with fire emissions

turned ON, while the sensitivity test for changing the initial emissions and using WRF-Chem

show differences of simulations turning smoke emissions on and off. These three sensitivity

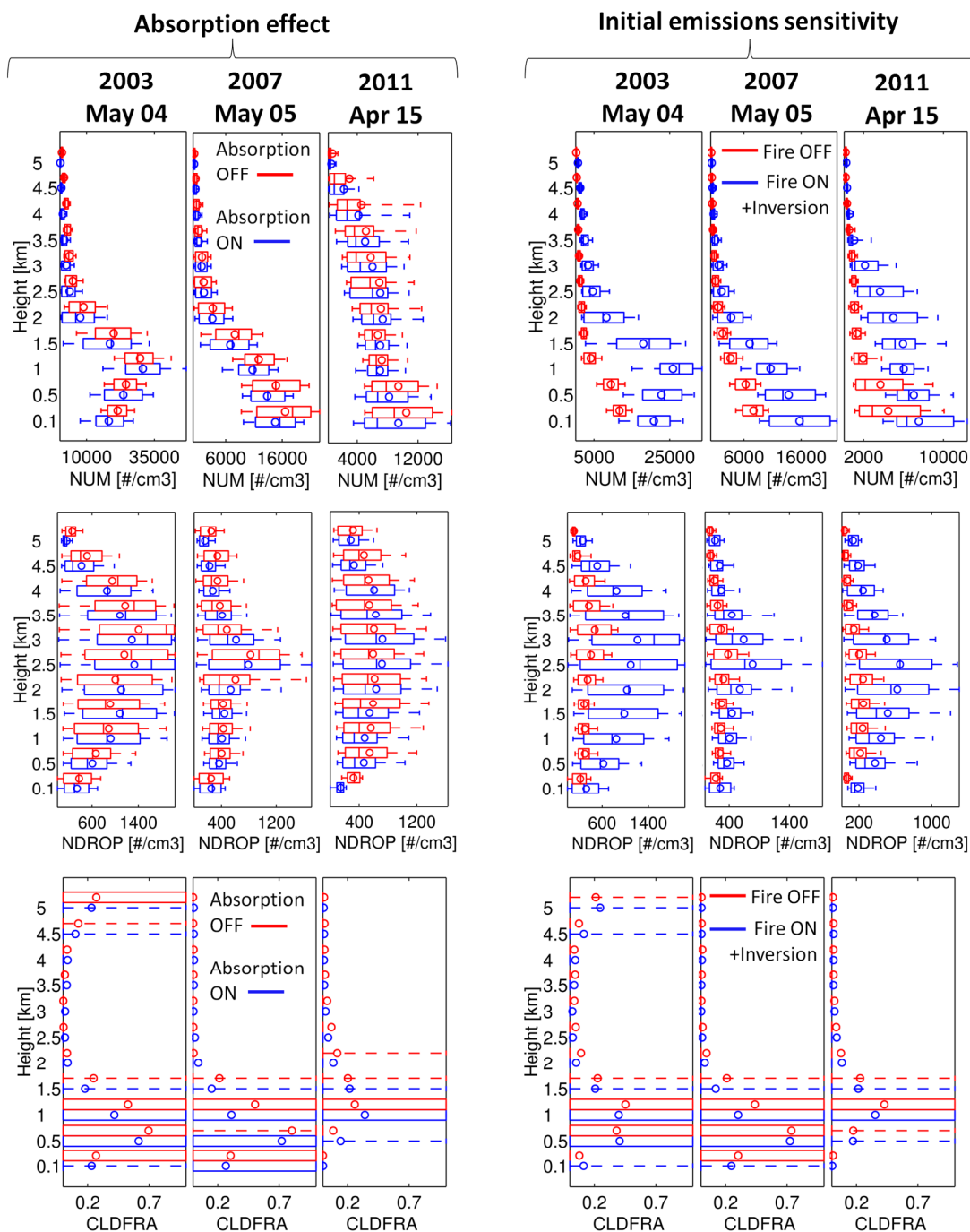cases are highlighted in Figure 9 for better comparison.

Figure 11. As Figure 7 for two sensitivity cases, turning off aerosol absorption (left panels) and

performing the inversion with a different set of initial biomass burning emissions (right panels).

See details of these simulations on the text. The left panels show a comparison of two

777   simulations with biomass burning turned on while the right panels compares simulations with

778   emissions turned on and off.
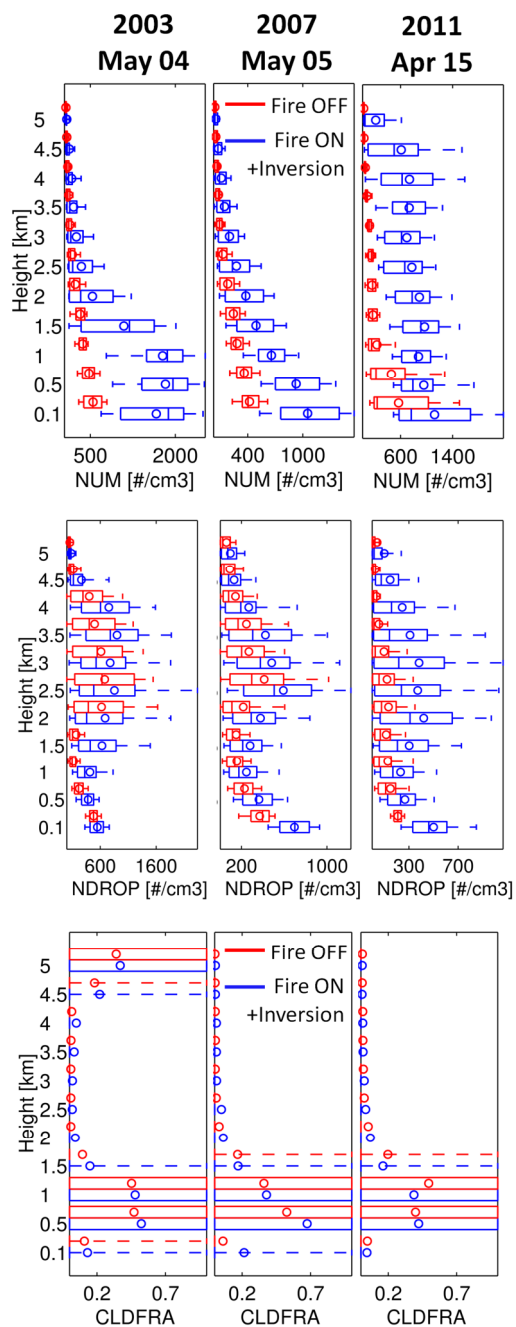
779

780   Figure 12. As Figure 7 but for WRF-Chem simulations. Aerosol number corresponds to the

781   accumulations mode (150-625 µm dry diameter)